Fuel 427 (2027) 140065

Contents lists available at ScienceDirect

Fuel

journal homepage: www.elsevier.com/locate/fuel

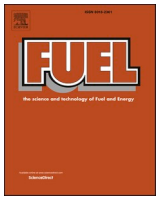

Full Length Article

Investigating OME_3-diesel droplet evaporation, combustion dynamics, and soot characterization☆

Farhad Mazari *, Thanos Megaritis

College of Engineering Design and Physical Sciences, Brunel University London, Uxbridge UB8 3PH, United Kingdom

ARTICLE INFO

Keywords:
Autoignition delay
Combustion duration
Droplet combustion
Oxygenated fuels
Oxymethylene ether (OME_3)
Soot formation
Ultrafine particles

ABSTRACT

The combustion behavior of fuel droplets plays a crucial role in controlling emissions and combustion efficiency in internal combustion engines. Droplet heating, evaporation, and burning characteristics strongly influence ignition delay, combustion duration, and soot formation. Oxymethylene ethers (OMEs), particularly oxymethylene ether-3 (OME_3), have attracted interest as drop-in diesel alternatives due to their high oxygen content and clean combustion potential. This study experimentally investigates the combustion of a single fuel droplet suspended on a thermocouple and exposed to a controlled environment at 500 °C and atmospheric pressure. Four fuels were examined: neat diesel and diesel blends containing 20, 40, and 60 vol% OME_3. High-speed imaging was used to analyze ignition delay, combustion duration, and flame luminosity, complemented by scanning electron microscopy (SEM) of collected particulates. Increasing OME_3 content significantly reduced ignition delay (by ~ 65–70% for D40-O60) while increasing combustion duration by ~ 25–30%. Flame luminosity decreased markedly, indicating suppression of macroscopic soot. This behavior is primarily attributed to the high oxygen content of OME_3, which promotes oxidation pathways that limit soot precursors formation. SEM analysis revealed a shift toward finer particles, with sub-micrometer particle counts increasing from ~ 120 mm^{-2} to ~ 340 mm^{-2}. These results demonstrate that reduced flame luminosity does not necessarily correspond to lower particulate emissions but instead reflects a shift toward ultrafine particle formation. Overall, OME_3 modifies combustion behavior by reducing visible soot while increasing ultrafine particle number density, highlighting a critical trade-off in oxygenated fuel performance.

1. Introduction

Diesel spray combustion includes fuel–air mixing, ignition, and combustion duration. These processes govern fuel vaporization, mixing, and oxidation reactions, thereby influencing both performance and emissions. To reduce emissions and maintain efficiency, various additives have been evaluated. These include cetane improvers, oxygenates such as ethanol and di-n-butyl ether, and metal-based compounds like ferrocene and cerium oxide. These additives improve ignition quality and combustion and reduce soot [1–4]. Oxygenated additives are especially promising for enhancing oxidation of soot precursors [5]. This effect is primarily attributed to the presence of chemically bound oxygen, which promotes the formation of OH and O radicals during combustion, enhancing oxidation of soot precursors and inhibiting the growth of polycyclic aromatic hydrocarbons (PAHs), key intermediates in soot formation [6]. Still, the mechanisms by which oxygenates affect soot during diesel combustion remain insufficiently understood. This

☆ NOVELTY AND SIGNIFICANCE STATEMENT*A droplet-scale combustion framework was developed to capture the full fuel droplet life cycle, including evaporation, autoignition, flame development, and soot formation. Optical flame diagnostics were combined with post-combustion airborne particle analysis to directly link ignition delay, combustion duration, and droplet thermal evolution with particle-resolved soot characteristics. The results reveal a systematic shift in soot evolution with increasing OME_3 content, where altered ignition and burning dynamics suppress large soot agglomerates while promoting ultrafine and sub-micrometer particle formation. Although the tendency of oxygenated fuels to increase ultrafine particles has been reported in prior studies, this work uniquely demonstrates how these trends originate from changes in droplet-scale evaporation-combustion coupling and flame structure under controlled single-droplet conditions. This demonstrates that reduced flame luminosity does not necessarily correspond to lower particulate emissions and may instead indicate a redistribution of soot toward finer particle sizes. These findings provide mechanistic insight into the competing roles of nucleation, growth, and oxidation processes in oxygenated fuel combustion. The results highlight the role of fuel-bound oxygen in enhancing soot precursor oxidation, inhibiting agglomeration growth, and reshaping soot formation pathways, emphasizing the need for integrated optical and particulate diagnostics when evaluating combustion performance and emissions characteristics.*

* Corresponding author.
E-mail address: farhad.mazari@brunel.ac.uk (F. Mazari).

https://doi.org/10.1016/j.fuel.2026.140065
Received 26 March 2026; Received in revised form 5 May 2026; Accepted 25 May 2026
Available online 28 May 2026

Nomenclature

Parameters

D	Diesel
NOx	Nitrogen Oxides
O	Oxymethylene Ether
OME	Oxymethylene Ether
OME_3	Oxymethylene Ether3
DBE	Di-n-butyl Ether

Abbreviations

CI	Compression Ignition
EHC	Electrically Heated Catalytic
EOC	End of Combustion
FPS	Frames Per Second
IDT	Ignition Delay Time
LTO	low-temperature oxidation
NTC	Negative Temperature Coefficient
PRF	primary reference fuel
ROI	Region of Interest
SEM	Scanning Electron Microscope
SOC	Start of Combustion
TC	Thermocouple

work investigates how oxymethylene ether additives, at the droplet scale, influence soot formation pathways and particulate characteristics. It also explores how they alter combustion dynamics and particulate emissions.

Oxymethylene ether (OME) is a synthetic oxygenated fuel composed of repeating CH_2-O units, with the general chemical formula H_3C-O-(CH_2O)n-CH_3. OMEs are typically produced as mixtures following a Flory-Schulz distribution, resulting in a range of chain lengths rather than a single pure compound [7]. In the OME series, OME_3 (n = 3) stands out for its high oxygen content and optimal volatility [8–11]. These features make it effective for supporting reduced soot formation and more efficient oxidation processes. Shorter-chain OMEs (OME_1 and OME_2) exhibit good volatility but present storage and ignition challenges [12]. Longer-chain OMEs (OME_4 and OME_5) have poor evaporation characteristics [13–15]. OME_3 vaporizes efficiently and provides reliable ignition, so it blends well with diesel and promotes stable flame development [16]. The absence of carbon-carbon (C-C) bonds in OMEs suppresses the direct formation of C_2 hydrocarbon fragments, which are essential precursors for aromatic species and soot formation. As a result, soot formation is significantly reduced; however, soot is not entirely eliminated, as it may still arise from recombination reactions of intermediate radicals under certain conditions. However, recent studies indicate that while soot agglomeration is reduced, oxygenated fuels may promote the formation of ultrafine particles, highlighting a potential trade-off in particulate emissions. Its molecular structure, consisting only of C-H, C-O, and O-H bonds, enables rapid autoignition, controlled combustion, and improved emission profiles [17]. These advantages make OME_3 suitable for reducing soot output, supporting cleaner engine operation, and enhancing overall performance when blended with diesel.

Recent research involving 10% OME_3-diesel blends has demonstrated notable improvements in combustion and emission control [18]. For example, Mazari [19] reported a 78.2% reduction in soot emissions and a faster start of combustion (SOC) for neat OME_3 compared to conventional diesel. Haspel et al. [14] observed shorter ignition delays at higher OME_3 concentrations, attributed to increased fuel reactivity, greater oxygen availability, and unique spray-flame structures that facilitate efficient ignition and combustion. This finding suggests that increasing OME_3 content modifies combustion behavior and emission characteristics. He et al. [20] further confirmed that OME_3 exhibits shorter ignition delay times and lower soot emissions than diesel, with additional validation from shock tube studies by Cai et al. [21]. Pélerin et al. [22] demonstrated that soot emissions were significantly reduced, and low particle numbers were maintained at high exhaust gas recirculation (EGR), supporting the application of OME_3 in heavy-duty engines. These studies highlight the potential of OME_3 blends in reducing emissions while maintaining engine performance.

Wang et al. [23] found that blending 25% OME_3 with n-heptane enhanced low-temperature oxidation (LTO) and highlighted a negative temperature coefficient (NTC) effect. Moreover, Chen et al. [24] focused on the LTO behavior of OME_3 blended with diesel and gasoline surrogates, using a blend of 30% OME_3 and 70% gasoline/diesel. They found that OME_3 significantly advanced the onset of low-temperature heat release and increased intermediate species formation during the NTC region, thereby improving overall reactivity. This showed the chemical efficiency of OME_3 blends under different combustion conditions. Evidence from [25–29] highlights OME_3's ability to reduce soot and emissions while improving both macroscopic combustion behavior and microscopic soot structure evolution. These findings support the potential of OME_3 for reducing soot emissions under certain conditions. However, few studies have examined particulate emissions at the droplet scale. Previous droplet combustion studies of oxygenated fuels such as alcohols, esters, and ethers have demonstrated similar trends in soot suppression and altered evaporation behavior, indicating that both physical and chemical effects govern combustion characteristics [6,11]. Comprehensive analysis of particle number, size, and morphology is critical to understanding OME_3's impact on soot pathways. Combining optical droplet observations with air sampling and SEM analysis quantifies total particle and ultrafine (<1 μm) fractions. This links flame dynamics with particulate formation and provides insight into the competing roles of nucleation, surface growth, agglomeration, and oxidation in soot evolution.

To better understand the broader engine-scale relevance of these findings, it is essential to connect droplet-scale observations with larger combustion dynamics. Insights gained from droplet-scale studies can inform the assumptions and boundary conditions used in engine-scale models. However, droplet studies do not fully capture high-pressure, turbulent, and multi-droplet interactions characteristic of engine environments. Such interactions include turbulence and varying thermodynamic conditions. Additionally, the present configuration involves a fuel droplet supported on a thermocouple and exposed to buoyancy-driven convection, which differs from idealized free-floating droplet combustion and should be considered when interpreting quantitative results [30,31]. Improving the integration between droplet-scale phenomena and engine-scale modeling will enhance our ability to predict and optimize emissions in practical applications.

Although earlier research examined ignition delay and soot reduction, droplet-scale combustion of OME_3-diesel blends at high temperatures remains poorly studied. It is necessary to systematically compare blend ratios from preheating to soot formation. This will clarify how visible flame luminosity relates to sub-micrometer particle formation. While previous single-droplet studies have addressed individual oxygenates [30,31], comprehensive investigations of OME_3-diesel blends are now emerging. These studies contribute to clarifying the impact of OME_3 on particulate formation under engine-relevant conditions [32–37]. To address this gap, high-speed optical imaging was employed to examine OME_3-diesel droplet combustion at 500°C under atmospheric pressure conditions. Pure diesel and blends containing 20, 40, and 60 vol% OME_3 were studied to provide a systematic basis for comparison.

The objective was to capture evaporation, ignition, flame development, and soot formation under controlled conditions. Airborne particulate matter was collected using a controlled air sampling system with quartz filters and analyzed via SEM. The particle number, density, and size were assessed. Although single-droplet combustion does not fully

replicate complex spray dynamics in engines, it provides fundamental insights into key phenomena at the droplet level. This dual approach, linking droplet-scale flame dynamics with particle characterization, not only enhances understanding of OME_3's role in soot evolution but also provides a more comprehensive understanding of soot evolution and highlights the trade-off between reduced visible soot and increased ultrafine particle formation in oxygenated fuel combustion.

2. Methodology

A thermocouple-supported droplet combustion optical setup was used to study fuel-dependent evaporation, ignition, flame evolution, and soot formation under controlled high-temperature conditions. High-speed optical diagnostics were combined with airborne particulate sampling and SEM analysis to link droplet combustion behavior with particle-scale soot characteristics. It should be emphasised that the present configuration represents a non-spherical, thermocouple-supported liquid mass rather than a freely suspended droplet. The combustion process is therefore influenced by thermocouple conduction, support effects, and buoyancy-driven natural convection. As a result, the data are interpreted in a comparative and qualitative framework and therefore should not be directly extrapolated to free-floating droplets or engine conditions.

2.1. Setup and configuration

The key controlled parameters in all experiments were as follows: the temperature was consistently maintained at approximately 500°C, the droplet diameter was standardized at 1.5 mm, and each test was repeated 7 times to ensure reliability. The chamber operated at atmospheric pressure (≈1 atm), and natural convection was present due to buoyancy effects at elevated temperature.

The experimental setup, illustrated in Fig. 1, consists of a tube surrounded by a PID-controlled heater and sealed at both ends with quartz glass, enabling optical measurements using a high-speed Photron SA-X2 camera. A high-power LED and diffuser plate are positioned behind the tube for shadowgraph imaging. The PID controller maintains the temperature within ±5°C, as verified by calibrated K-type thermocouples (three thermocouples positioned axially and radially within the furnace to ensure spatial uniformity). The system is stabilized for at least 30 minutes prior to testing to ensure uniform thermal conditions.

Droplets are suspended on a thermocouple and introduced via a traversing mechanism. The droplet was supported on a K-type thermocouple junction formed as a fine bead with a diameter of approximately 0.2 mm, created by welding twin-twisted wires. This small junction size was selected to minimise physical interference with the droplet while maintaining reliable temperature measurement at the droplet location. The thermocouple was oriented horizontally to ensure consistent droplet placement and to reduce asymmetry induced by gravitational effects. The presence of the thermocouple introduces a conductive heat transfer pathway that can influence droplet heating and evaporation behavior. In addition, variations in fuel properties such as surface tension and wettability may alter the contact area between the droplet and the thermocouple junction. However, all experiments were conducted

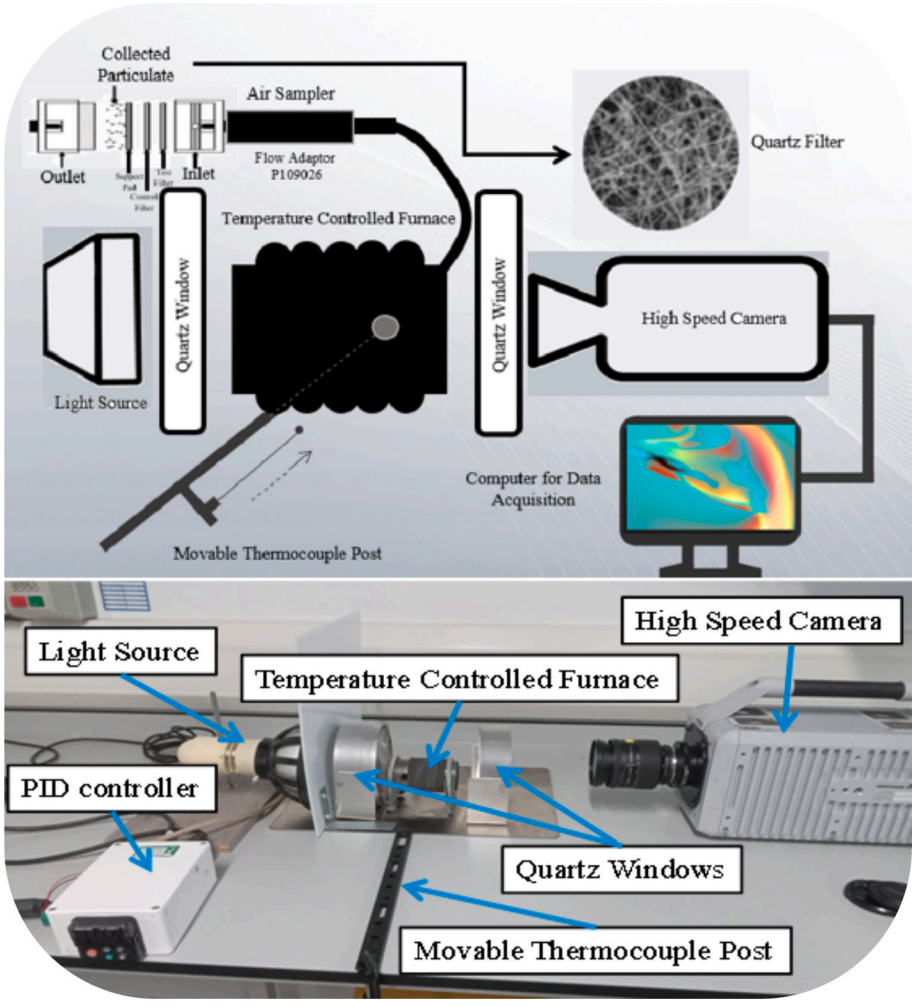

Fig. 1. Experimental setup for studying Diesel-OME_3 combustion characteristics.

using the same thermocouple configuration and identical operating conditions across all fuel blends.

Therefore, while the absolute heat transfer may be affected by the support configuration, the comparative trends between fuels remain consistent and reliable. Although no explicit correction factor is applied, the thermocouple influence is treated as a systematic effect and therefore does not compromise the relative comparison between different fuel blends. The magnitude of conductive heat transfer through the thermocouple is expected to be small due to the relatively low cross-sectional area of the junction compared to the droplet volume; however, it may influence early-stage heating rates. The small thermocouple diameter relative to the initial droplet size (~1.5 mm) further limits its influence on the overall droplet combustion behavior. The insertion process occurs over approximately 0.3 s, which may induce a transient relative gas flow around the supported liquid mass; this effect is consistent across all tests and is therefore treated as a systematic condition. The thermocouple tip holds 1.6 μL of fuel, providing sufficient mass for evaporation and rapid thermal response. High-speed imaging is conducted at 12,500 fps, with a 1.25 μs exposure time and 728 × 728-pixel resolution, capturing droplet dynamics and combustion processes.

The experimental configuration aligns with established methodologies carried out in this setup, as demonstrated in prior work [11,38,39]. Commercial diesel fuel was used in this study; however, it is acknowledged that diesel composition can vary depending on source and season. The reported properties, therefore, represent typical ranges rather than a fully defined surrogate composition, which may limit direct applicability for detailed chemical modeling.

The distinct chemical properties of diesel and OME_3 used in this work are summarised in Table 1. All blend ratios (e.g., D80-O20, D60-O40) are defined on a volumetric basis (vol%). In addition to optical diagnostics, an air-sampling system was incorporated to quantify particulate matter generated during combustion. A Casella Apex2 pump with matched-weight cassettes containing 20 μg tolerance quartz filters was positioned adjacent to the metallic cube housing the heater to collect airborne particles within the measurement zone. Quartz filters were selected due to their high purity and resistance to thermal degradation, making them well-suited for diesel particulate analysis. Air was drawn through the system at a constant flow rate of 5 L/min, with particulates deposited onto the primary test filter while a secondary filter beneath served as a blank control. Following sampling, both filters were equilibrated under controlled conditions and subsequently analyzed to estimate the collected particulate mass through pre- and post-sampling filter measurements. The layout of this sampling arrangement is shown in Figs. 1 and 2.

It should be noted that the present study is conducted under simplified droplet-scale conditions (atmospheric pressure and natural convection), and therefore, the results are intended to provide fundamental insights into fuel-dependent combustion behavior rather than direct quantitative representation of practical engine environments.

Table 1
The chemical properties of diesel and OME_3 were utilised in this study [40].

Parameter	Diesel	OME_3
Molecular Structure	C_mH_n ($<C_8H_{18}$)	$C_5H_{12}O_4$
Oxygen Percentage (*wt. %*)	0	47
Heating Value (*kJ/g*)	43	19
Flashing Point (°*C*)	>55	88
Cetane Number –	>51	84
Boiling Range/ Characteristic Boiling Point (°*C*)	180–390	202
Viscosity (40°C) (*mm^2/s*)	2–4	1.33
Density (g/cm^3 at *T_{st}d*)	0.82–0.85	1.1–1.15
Surface Tension (mN/m at room *T*)	25–35	20–30

Note: Heating values correspond to lower heating value (LHV). Diesel exhibits a broad boiling range due to its multi-component composition, whereas OME_3 behaves more like a single-component fuel, with a narrower volatility range.

2.2. SEM analysis of airborne particulates

The collected samples were further analyzed to quantify airborne particulates captured on the quartz-filter cassettes using a bias-minimizing protocol. Bright-field SEM imaging was carried out from low magnification up to ×2500, with particles identified across multiple fields of view, yielding a representative subset of particles per sample. Particle identification and counting were performed using image thresholding and manual verification to minimize operator bias.

Across each filter, 100 fields of view at ×2500 magnification were examined, corresponding to a minimum observed area of 1.079 mm^2. Particle density on the filter surface was calculated as D = n/t, where n is the number of particles counted, t is the analyzed area in mm^2, a is the effective filter area, and V is the sampled air volume. While particle concentration per millilitre of filter eluate was defined as C = (n×a)/(t×V), where a is the effective filter area and V is the air volume sampled. The analytical sensitivity of the method was given as S = a/(t×V) where all variables are defined consistently above.

It should be noted that SEM measurements represent two-dimensional projections of particles deposited on the filter surface, and therefore, particle size is reported as an equivalent projected diameter rather than a true three-dimensional metric. These measurements enabled direct comparison of particle formation under the tested combustion conditions and provided specific insight into the prevalence of sub-micrometer fractions observed in the SEM images.

While efforts were made to improve statistical representativeness by sampling 100 fields of view across each filter, the analyzed area (~1.079 mm^2) represents only a small fraction of the total filter surface (25 mm diameter). Therefore, the reported particle counts should be interpreted as representative of local sampling regions rather than absolute filter-wide distributions. Additionally, no full particle size distribution or uncertainty analysis was performed; thus, the results are primarily intended for comparative assessment between fuel blends under consistent experimental conditions. These metrics represent surface-based particle number density rather than time or mass-resolved emission rates.

2.3. Image processing

Acquired high-speed images were processed using a custom MATLAB-based code. An equivalent droplet diameter was determined by evaluating the projected cross-sectional area, after background subtraction to isolate the droplet, followed by binarization. The equivalent diameter (Deq) was calculated by assuming a circular projection with the same area as the segmented liquid region. This definition provides a consistent metric for comparison, although the droplet deviates from spherical geometry due to thermocouple support and gravity. The initial droplet size was recorded as a baseline, and subsequent effects of evaporation were quantified by tracking changes in projected area. To minimize the influence of initial droplet-size variability across experiments, all droplet-evolution data are presented in normalized form (D/D_0), where D_0 denotes the initial equivalent droplet diameter. To ensure the reliability of the results, each fuel blend was tested seven times under identical conditions. Temporal fluctuations (e.g., oscillations in Deq^2 trends) are attributed to multi-component evaporation effects, including preferential vaporization and internal boiling phenomena. The camera settings in this setup yielded a spatial resolution of 25 μm per pixel.

The spatial resolution introduces an inherent measurement uncertainty of approximately ±1 pixel in edge detection, corresponding to ±25 μm in the equivalent droplet diameter. For a typical initial droplet diameter of ~1.5 mm, this yields a relative uncertainty of approximately ±1.7%. Additional uncertainty may arise from image thresholding during binarization and slight variations in droplet shape due to the thermocouple support. These effects are mitigated by repeated experiments and averaging across seven trials for each fuel condition.

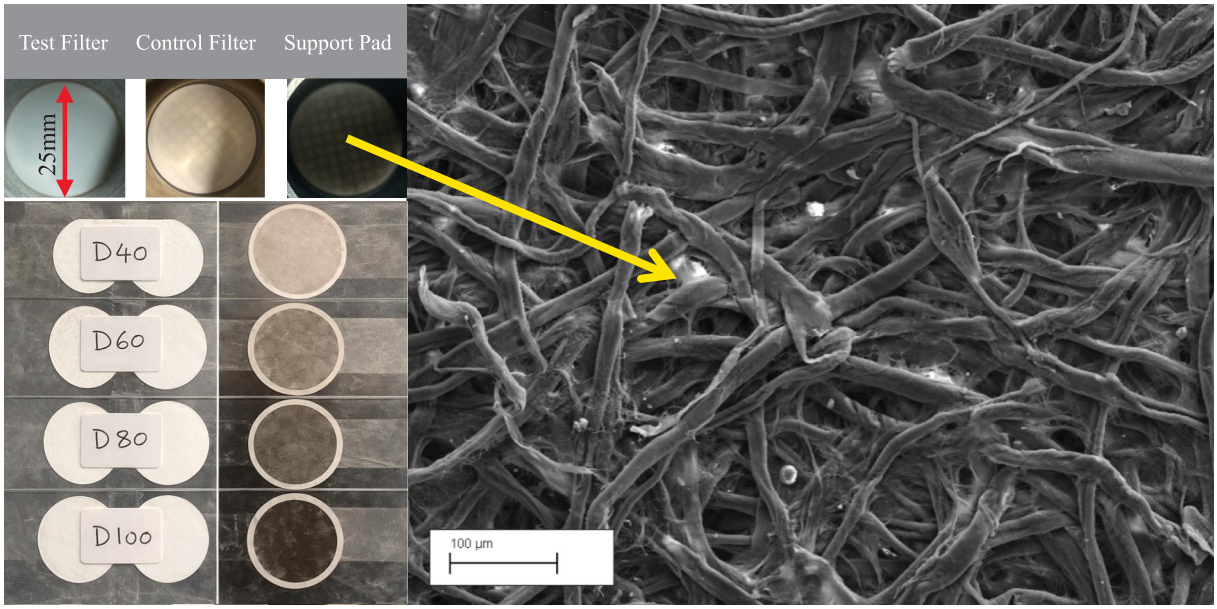

Fig. 2. Quartz filter sampling and SEM imaging of particulates from OME_3-diesel blends.

3. Results and discussion

3.1. Pre-combustion droplet size evolution

This section examines the evaporation dynamics of various fuel compositions, including pure diesel (D100) and blends with different concentrations of oxymethylene ethers (OME_3): D80-O20, D60-O40, and D40-O60. The primary objective is to evaluate how variations in fuel formulation affect droplet evaporation and combustion characteristics. The initial droplet size was measured from images captured at the moment the droplet reached the center of the furnace. During the pre-ignition heating phase, all droplets exhibited a reduction in initial size prior to combustion, as shown in Fig. 3A-G, highlighting the critical role of evaporation and mixing in preparing the droplet for ignition and efficient combustion. This size change was quantified through frame-by-frame image analysis before flame appearance.

This finding suggests that incorporating oxymethylene ethers into diesel blends can enhance fuel evaporation and combustion efficiency, thereby improving engine performance and reducing emissions.

All four fuel blends exhibited distinct droplet evaporation rates at the initial instant of observation (Fig. 3A), where the droplets appeared stable. Subsequently, a gradual reduction in normalized droplet diameter was observed (Fig. 3B) due to heat transfer from the surrounding environment to the droplet core during the early heating phase. A transient increase in normalized droplet diameter (D/D_0) in subsequent frames (3C and 3D) is observed, which is attributed to internal vapor generation and droplet swelling. This behavior arises from the preferential evaporation of more volatile components present in both diesel and OME_3, rather than being solely associated with OME_3. This behavior is characteristic of multi-component fuels, where volatile fractions

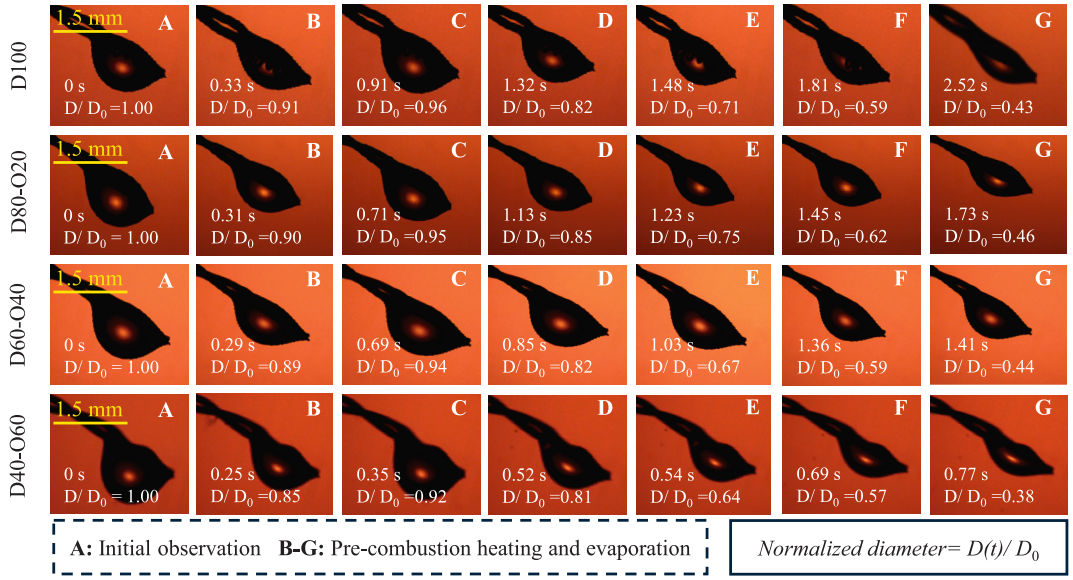

Note: *D_0 is the initial equivalent droplet diameter measured at 0 s (frame A) for each test.*

Fig. 3. Optical sequence of droplet behavior during pre-combustion. Normalized droplet diameter (D/D_0) is provided for each frame, obtained from image processing of the projected droplet area.

vaporize first, causing internal pressure buildup and transient swelling [41]. As shown in Table 1, diesel exhibits a wide boiling range (180-390 °C), indicating the presence of both light and heavy fractions, whereas OME_3 has a narrower and more defined boiling characteristic around 202 °C. This difference in volatility distribution supports the observed multi-component evaporation behavior, where both diesel light fractions and OME_3 contribute to transient droplet swelling. Although detailed distillation curves were not measured in this study, the observed trends are consistent with reported volatility characteristics of diesel and oxygenated fuels. Minor variations in droplet shape are attributed to differences in surface tension and wettability at the thermocouple junction. However, these variations were consistent across repeated experiments and do not affect the comparative analysis, as droplet size is quantified using an equivalent diameter based on projected area.

As thermal decomposition progresses, the droplets enter a rapid evaporation phase (3E), eventually stabilizing in size (3F) before combustion (3G). The reported "diameter" is an equivalent diameter derived from the projected cross-sectional area of the supported droplet, rather than a true spherical diameter, due to deformation induced by thermocouple support and gravity. These temporal changes align with the normalized droplet-diameter-squared profiles shown in Fig. 4, highlighting the significant influence of fuel composition on evaporation dynamics.

Although normalized droplet diameter-squared ($(D/D_0)^2$) trends are presented in Fig. 4 to facilitate comparison of evaporation behavior across fuels, it should be noted that the classical D^2-law is not strictly applicable under the present experimental conditions. This is due to the multi-component nature of diesel-OME_3 blends, transient heating, internal boiling effects, and droplet deformation induced by thermocouple support. These factors lead to non-linear evaporation behavior, deviating from the quasi-steady, single-component assumptions underlying classical droplet combustion theory. Therefore, the analysis in this study focuses on comparative evaporation and combustion trends rather than the extraction of a single burning rate constant.

The image sequences presented are representative of repeated experiments conducted under identical conditions. While minor variations exist between trials, consistent trends were observed across all repetitions; quantitative variability is reported separately where applicable.

The droplet profiles depicted in Fig. 4 demonstrate that the evaporation behavior of fuel droplets is strongly governed by their chemical composition, particularly the proportion of oxygenated components due to the presence of OME_3. Blends with a higher diesel fraction exhibited prolonged evaporation times, primarily due to the higher boiling points and lower volatilities of diesel components, as also noted in studies on multi-component fuel evaporation behavior, such as that by Pitsch et al. [42]. Conversely, as OME_3 content increased, droplets exhibited a more rapid rate of size reduction over time, consistent with steeper $(D/D_0)^2$ decay trends observed in Fig. 4. This behavior can be attributed to the enhanced volatility of OME_3-rich blends, which stems from their lower boiling range and elevated vapor pressure.

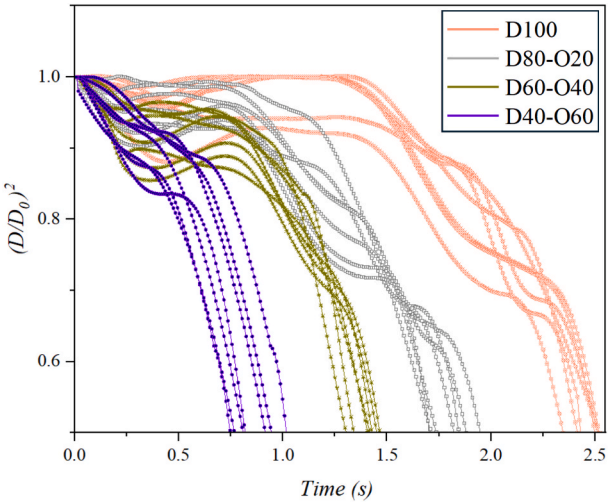

Fig. 4. $(D/D_0)^2$ curves during pre-combustion evaporation.

Although a single linear burning rate constant cannot be rigorously extracted due to the non-linear evaporation behavior observed, qualitative comparison of the slopes of the normalized droplet diameter-squared ($(D/D_0)^2$) curves in Fig. 4 provides useful insight into relative evaporation rates among the fuel blends. In classical droplet combustion theory, a linear decrease in D^2 with time indicates a constant burning rate; however, the present results exhibit deviations from linearity, particularly during the early heating and swelling phases. Despite this, the overall trend shows that OME_3-rich blends display steeper reductions in $(D/D_0)^2$ during the main evaporation phase, indicating higher effective evaporation rates compared to pure diesel. This behavior is attributed to the higher volatility and oxygen content of OME_3, which promote rapid vaporization and more efficient fuel-air mixing. Therefore, while a strict D^2-law analysis is not applicable, the observed trends are consistent with an increase in effective burning intensity with increasing OME_3 content.

3.2. Combustion dynamics

Fig. 5 illustrates the combustion sequence following the evaporation phase shown in Fig. 3. The sequence tracks the combustion process from the first visible flame to completion for each fuel blend. It reveals key differences in autoignition delay, flame luminosity, combustion duration, and soot formation among pure diesel (D100) and OME_3-diesel blends, including D80-O20, D60-O40, and D40-O60. Due to strong flame luminosity, the droplet boundary becomes obscured after ignition, preventing reliable extraction of droplet diameter during the combustion phase.

In the case of pure diesel (D100), the autoignition process was abrupt, leading to a rapid expansion of the flame front as a significant fraction of the droplet had already transitioned to the vapor phase before ignition, resulting in a rapid expansion of the flame front and a strong premixed combustion component during the early stage of combustion. By 2.85 seconds, the flame exhibited reduced luminosity and was displaced downstream. This shift could be attributed to fuel-rich conditions and local oxygen depletion, leading to a less luminous combustion, as similarly observed in studies examining fuel-rich combustion environments [43]. At 3.11 seconds, this behavior led to early soot formation, as indicated by the emergence of dark, dense regions within the flame, which persisted throughout the combustion phase, consistent with observations reported by Nobili et al. [44] for soot generation under fuel-rich or incomplete combustion conditions. At 3.36 seconds, the flame appeared to regain intensity, with noticeably less surrounding soot, suggesting a brief resurgence in combustion activity. By 3.52 seconds, the flame diminished significantly, entering its final phase before extinction. At 3.62 seconds, the flame extinguished abruptly, leaving behind a visible soot trail, suggesting incomplete combustion.

Following the baseline diesel experiment, OME_3 was blended with diesel at 20% by mass (D80-O20) to study its impact on combustion and soot formation. The addition of OME_3, with its higher cetane number and oxygen content, led to an earlier SOC relative to pure diesel, occurring at approximately 1.9 seconds. At this point, the flame behavior resembled that of pure diesel, with a stable and well-defined combustion zone. However, by 2.17 seconds, shortly after SOC, early soot formation was observed, with soot particles visible near the droplet, likely due to incomplete combustion in the fuel-rich zone. As combustion progressed, the flame luminosity decreased, likely due to soot particles absorbing emitted light. The droplet remained visible until around 2.45 seconds, indicating prolonged liquid-phase fuel presence

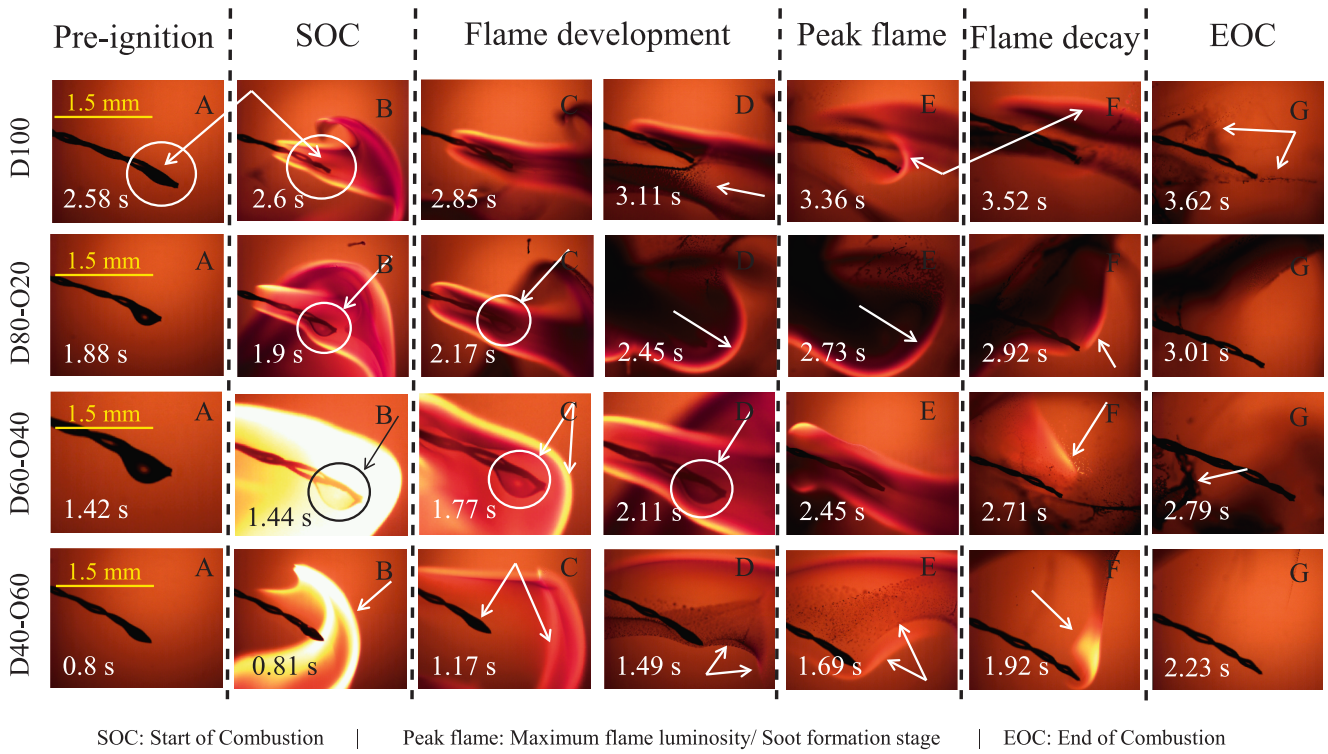

Fig. 5. Droplet combustion sequence of diesel-OME_3 blends. Frames (A-G) represent key combustion stages: pre-ignition, (SOC), flame growth, flame development, peak flame luminosity and soot formation, flame decay, and (EOC).

and a more gradual evaporation process, consistent with the extended combustion duration observed for this blend. Despite the smoke, the flame remained active until 2.92 seconds, as indicated by a bright orange glow surrounding the smoke. The flame extinguished abruptly with visible smoke at 3.01 seconds, indicating incomplete combustion, as smoke typically signifies soot formation due to insufficient oxygen for complete oxidation. This behavior was more pronounced in the D80-O20 blend compared to pure diesel, which exhibited a more rapid vaporization and earlier transition to fully developed combustion. A key distinction is that in pure diesel, the droplet evaporates early, before significant combustion begins, enabling a more complete oxidation. In contrast, the droplet in the D80-O20 blend remained visible until later in the combustion phase, indicating prolonged fuel presence and delayed vaporization, which contributes to localized fuel-rich regions and increased soot formation despite the longer overall burning duration.

Subsequently, an additional 20% OME_3 was blended into the mixture, forming the D60-O40 fuel. The droplet remained visible throughout the combustion process until the EOC, indicating a more stable and sustained burning phase. The SOC occurred at about 1.44 seconds, earlier than in both D100 and D80-O20, and was accompanied by a distinct luminous envelope, indicating a more reactive mixture promoting earlier ignition and improved oxidation. By 1.77 seconds, the central flame region appeared more intense, surrounded by a visible orange-hued luminous zone, indicating intensified combustion reactions. From 2.11 to 2.45 seconds, a displaced flame front was observed, similar to the transient flame displacement behavior seen in the D80-O20 blend at 2.17 seconds and in pure diesel at 2.85 seconds, indicating a period of dynamic flame movement before reaching the EOC at 2.71 seconds. While soot was less prominent during combustion in this mixture than in D80-O20 and diesel, it became noticeable at 2.79 seconds, though its level was much lower than that observed in both D100 and D80-O20 blends.

Next, an additional 20% OME_3 was added, forming the D40-O60 fuel. Unlike the previous blends, the liquid droplet was significantly reduced by 0.8 seconds, with most of the fuel existing as vapor mixed with the surrounding air. Visual observations indicate reduced and more dispersed soot presence, and more widely dispersed than with the other fuels, suggesting improved mixing, reduced soot formation, and enhanced oxidation.

Throughout the burn, the flame appeared relatively stable in shape and luminosity based on visual observation, with fewer abrupt fluctuations in size and intensity compared to lower OME_3 blends; however, this assessment is qualitative and based on image sequences rather than quantitative flame diagnostics. This behavior suggests a more uniform combustion process and improved flame stability relative to lower OME_3 blends, rather than implying strictly constant flame characteristics.

The SOC occurred at 0.81 seconds, much earlier than in previous tests. The longer combustion duration observed alongside earlier SOC is attributed to a more distributed and sustained heat release process, influenced by the lower heating value of OME_3, reduced soot radiation, and improved fuel-air mixing. These factors lead to a less localized combustion zone and a more gradual fuel consumption rate, thereby extending the overall burning duration despite enhanced oxidation conditions.

This is likely due to the higher oxygen content and improved fuel-air mixing associated with increased OME_3 concentration, which supported a steadier flame and prolonged combustion process, as similarly reported in studies examining oxygenated fuel blends by Lin et al. [45]. At 1.17 seconds, the flame region expanded and became less luminous, displaying a distinct outer diffusion zone with a visible yellow-orange flame. This shift in flame behavior suggests a transition from an initial phase involving localized premixed combustion, likely driven by rapid fuel vaporization and higher oxygen content, to a predominantly diffusion-controlled combustion mode for fuels with lower oxygen content. This transition is typical as the evaporation rate stabilizes, resulting in a more uniform and controlled flame structure, as also observed by Goroshin et al. [46]. Between 1.49 and 1.69 seconds, small soot particles were observed to be dispersed within the flame, which was still visibly active during this period, as indicated by the arrow in the image sequence. At 1.92 seconds, a brighter and more defined flame

emerged, marking the final stage of combustion. By 2.23 seconds, the flame had gradually faded, leaving only minimal soot.

Overall, increasing OME_3 content consistently modifies combustion behavior, with earlier ignition, extended burning duration, and reduced flame luminosity. These trends are attributed to enhanced fuel reactivity and the presence of fuel-bound oxygen, which promotes oxidation while limiting soot precursor formation, consistent with previous studies [17,47]. These trends are driven by OME_3's higher cetane number and inherent oxygen content, which enhance fuel reactivity and promote more complete oxidation while reducing soot precursor formation. The elevated cetane number reduces autoignition delay by accelerating low-temperature oxidation, while the oxygen content facilitates efficient hydrocarbon breakdown and suppresses soot precursor formation. Moreover, OME_3's higher volatility improves fuel-air mixing, leading to more homogeneous vapor distribution, uniform flame structures, and extended combustion durations. A notable observation in the OME_3-diesel blends is the prolonged presence of the fuel droplet in liquid form throughout most of the combustion process. Specifically, in the D80-O20 blend at 1.9 s and 2.17 s, in the D60-O40 blend at 1.77 s and 2.11 s, and in the D40-O60 blend at 1.17 s, the droplet remains visible.

In contrast, pure diesel droplets exhibit a longer pre-ignition phase followed by a sudden and intense ignition event, which leads to rapid combustion-driven vaporization and an apparent disappearance of the droplet around 2.6 seconds, consistent with observations in earlier studies of diesel combustion [48]. Although OME3 exhibits higher volatility, which enhances early-stage evaporation and promotes faster ignition, the subsequent combustion process becomes more distributed due to improved fuel-air mixing and the presence of fuel-bound oxygen. This results in a more gradual consumption of the fuel rather than rapid, localized vaporization. Consequently, droplet visibility persists for a longer duration, not due to slower evaporation, but due to a more distributed combustion process involving both liquid and vapor phases.

This distinction highlights that increased volatility primarily affects the pre-ignition and early combustion stages, whereas the balance between evaporation rate, heat release, and combustion dynamics governs the overall droplet lifetime.

As the fuel composition shifts from D100 to D40-O60, early flame brightness increases, likely due to improved ignition quality, stronger soot oxidation, and reduced soot formation. Flame luminosity then became more uniform, suggesting cleaner combustion with reduced particulate emissions, a trend also observed by Ilbas et al. [49]. Overall, increasing OME_3 content significantly improves combustion characteristics, modifies evaporation-combustion coupling, stabilizes flame behavior, and reduces soot formation.

3.3. *Impact of OME_3 Content on Soot Particle Characteristics*

The following analysis examines how varying OME_3 content in diesel fuel influences soot particle characteristics observed after combustion. All soot samples shown in Fig. 6 were collected at the end of combustion (EOC), defined as the point of visible flame extinction, to ensure a consistent comparison of soot morphology across all fuel blends. High-speed imaging reveals a transition from large, densely packed soot agglomerates in pure diesel to smaller, more dispersed particles as the OME_3 fraction increases. The observation scale (~200 μm) enables detailed comparison of soot morphology across fuel blends, as shown in Fig. 7.

Soot formation in droplet combustion involves nucleation, growth, agglomeration, and oxidation. In pure diesel combustion, the absence of fuel-bound oxygen promotes the formation of soot precursors (e.g., polycyclic aromatic hydrocarbons), which undergo surface growth and agglomeration to form large, chain-like soot structures. As the OME_3 content increases, oxygen within the fuel molecular structure enhances local oxidation reactions, suppressing surface growth and limiting the agglomeration of soot particles. At the same time, nucleation may still occur, forming smaller primary particles. However, these particles are more effectively oxidised before they can grow into larger aggregates. This results in a shift from fewer, larger soot agglomerates towards more numerous, finer particles, consistent with the observed soot morphology.

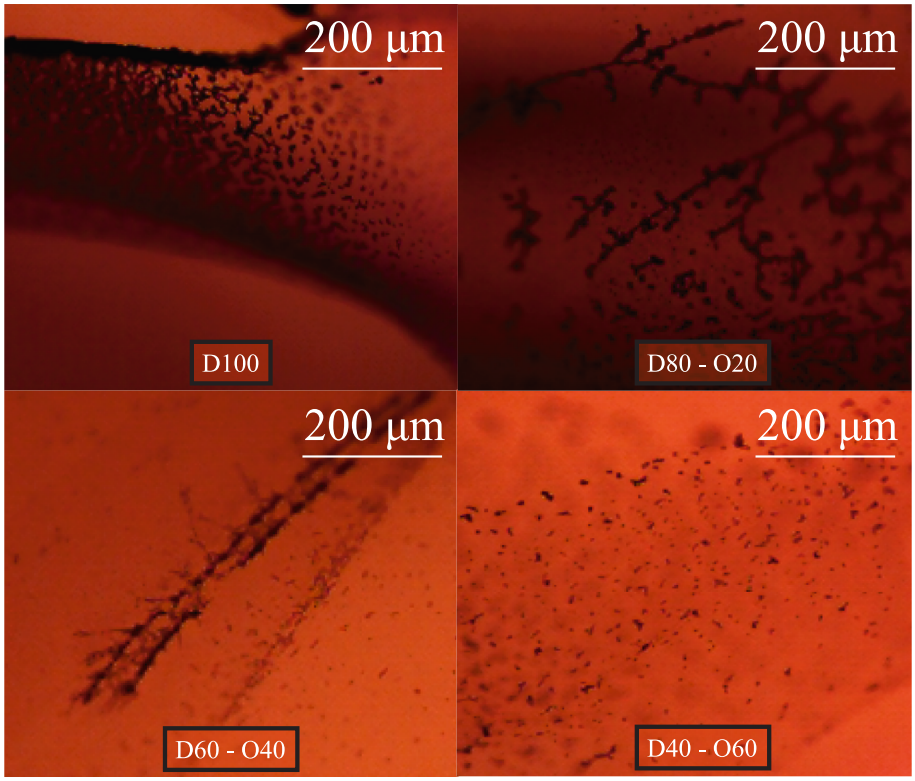

Fig. 6. Soot morphology from diesel-OME_3 blends at end of combustion (EOC).

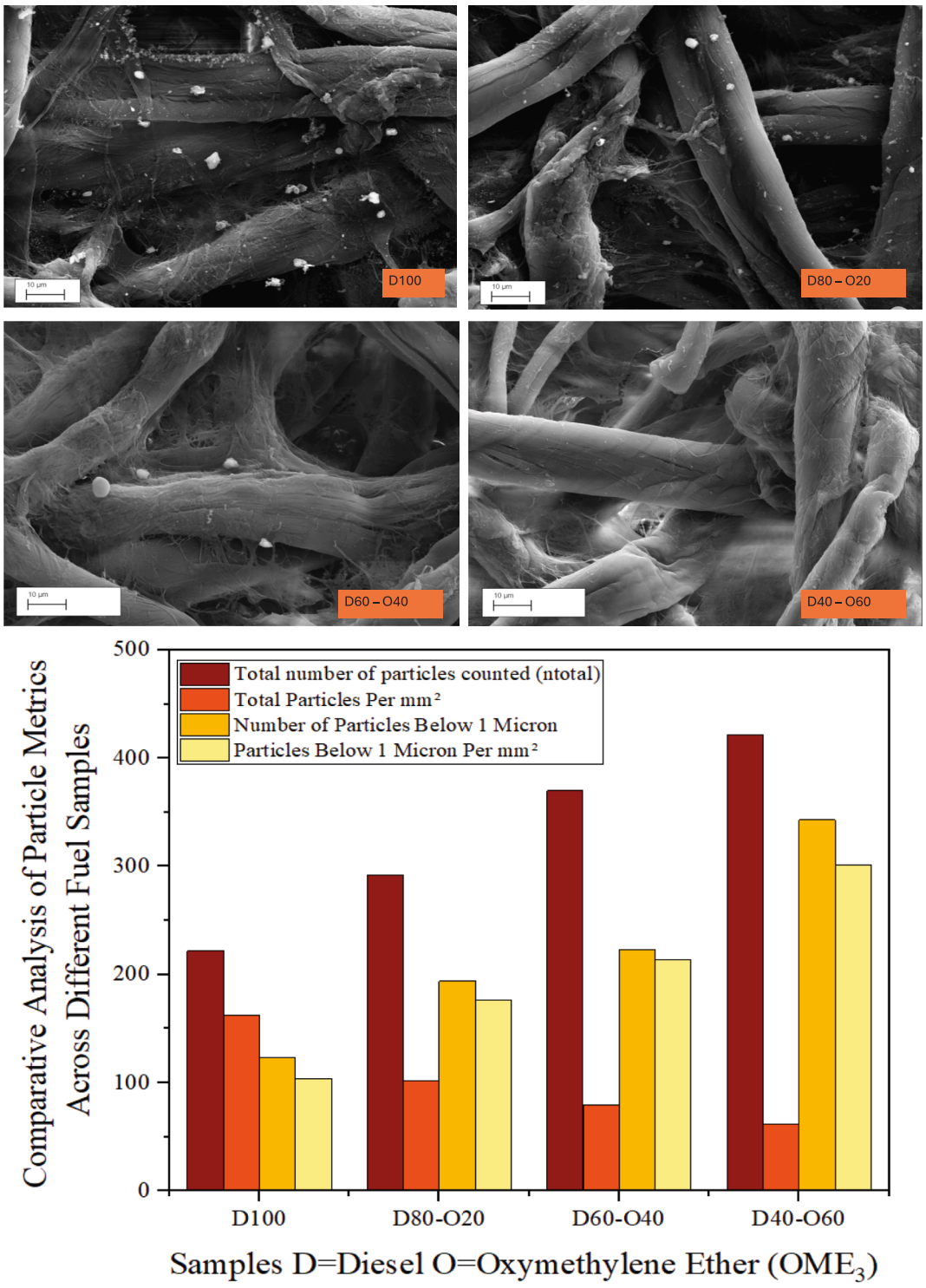

Fig. 7. Particle number metrics from SEM analysis of quartz filter samples.

In pure diesel (D100), soot particles form large, compact clusters with pronounced, chain-like branching structures. These extensive agglomerates result from incomplete combustion, where the absence of oxygenates limits the oxidation of soot precursors, leading to larger, more complex soot aggregates. Introducing 20% OME_3 (D80-O20) reduces the density and size of soot clusters, producing smaller and more fragmented particles, though some chain-like structures persist due to the relatively high diesel content. The additional oxygen from OME_3 enhances the oxidation of soot precursors, mitigating cluster growth. At 40% OME_3 (D60-O40), soot particles become noticeably finer and more dispersed, with less defined chain morphology, reflecting further improvement in combustion conditions. In the 60% OME_3 blend (D40-O60), soot particles are the smallest and most widely dispersed, exhibiting minimal aggregation. The high oxygen content enables more complete combustion, significantly lowering the extent of soot growth and agglomeration and resulting in predominantly small, near-spherical particles.

Overall, increasing OME_3 concentration in diesel reduces soot particle size and agglomeration while promoting finer particles, indicating enhanced soot oxidation and reduced particle growth, rather than

complete suppression of soot formation and a shift in particulate formation pathways with increasing oxygenate content.

3.4. Particle metrics of collected airborne soot

A notable phenomenon observed in this study is a 'paradox of cleaner flames.' While OME_3-rich blends reduce macroscopic soot emissions and visible flame luminosity, they simultaneously increase fine particulate matter. Fig. 7 summarises the SEM observations and quantitative particle metrics obtained from the previously shown airborne soot collected for the four fuel conditions (D100, D80-O20, D60-O40, and D40-O60). The reported particle numbers are normalized with respect to the analyzed filter surface area and are expressed as particle number per unit area (particles/mm^2). These values are not normalized by fuel mass burned or combustion time but instead represent spatial particle density measured under consistent experimental sampling conditions for all fuel blends. The results demonstrate a clear and systematic increase in particle counts as the OME_3 fraction increases. The total number of particles per minimum analyzed area of 1.079 mm^2 rises from 220 in D100 to 420-430 in D40-O60, representing almost a doubling of particle concentration across the fuel range. The sub-micrometer fraction (<1 μm) shows an even steeper increase, rising from 120 particles per 1.079 mm^2 in D100 to 340-350 particles per 1.079 mm^2 in D40-O60, which is a nearly 190% increase in the number of fine particles. This behavior is associated with the modification of soot formation pathways in oxygenated fuels, involving competing processes of particle nucleation, surface growth, agglomeration, and oxidation. The higher oxygen content in OME_3 enhances oxidation reactions and suppresses surface growth and agglomeration of soot particles, while simultaneously promoting the formation of smaller primary particles through increased nucleation rates. The higher oxygen content promotes oxidation processes that limit the growth and agglomeration of large soot structures, while simultaneously favoring the formation of smaller particles. Consequently, fewer large soot agglomerates are formed, but the number density of finer particles captured on the quartz filters increases significantly.

It should be noted that these particle counts are derived from a limited sampled area (~1.079 mm^2) and are based on two-dimensional projected measurements obtained from SEM imaging. As such, they do not represent full particle size distributions and may not fully capture spatial variability across the entire filter. Therefore, the reported values should be interpreted as comparative indicators of soot formation trends rather than absolute quantitative metrics.

These results highlight an important trade-off associated with oxygenated fuel blends. While increasing OME_3 content reduces visible soot formation and flame luminosity, it simultaneously increases the number density of ultrafine particles. This indicates that improved optical combustion characteristics do not necessarily correspond to reduced particulate emissions. From an application perspective, this trade-off is significant, as ultrafine particles are of greater concern for health and regulatory frameworks due to their ability to penetrate deep into the respiratory system. Therefore, combustion performance should be assessed using both macroscopic flame observations and particle-scale diagnostics to provide a more comprehensive evaluation of fuel behavior.

These findings reconcile the optical and SEM-based observations, providing a more complete understanding of how oxygenated additives modify soot formation pathways at the droplet combustion scale. Importantly, the increase in ultrafine particles raises potential health concerns, as these particles can penetrate deep into the respiratory system and have been associated with adverse cardiovascular and respiratory effects. This underscores the necessity for regulatory frameworks to consider both visible soot reductions and the implications of higher ultrafine particulate concentrations in assessing the overall environmental and health impacts of alternative fuel formulations.

3.5. OME_3 effect on ignition

As stated earlier in Section 3.1, the droplet was inserted rapidly, and the time between its initial deployment to the center of the camera's field of view was less than 0.3 seconds based on the average transition time measured across seven repeated tests. The ignition time was determined from the instant the droplet appeared fully stabilized at the center of the frame to the point of sustained flame development. The variation in ignition delay time is influenced by the thermo-physical and chemical properties of fuel mixtures, such as boiling point, surface tension, and cetane number, as shown in Fig. 8. Fuels with higher boiling points tend to evaporate more slowly, resulting in relatively longer ignition times, a trend also noted by Farooq et al. [50]. The addition of OME_3 significantly shortened the ignition time across all tested blends.

The blend containing 60% OME_3 and 40% diesel exhibited the shortest ignition time, achieving a 65.82% reduction compared to pure diesel. Blends with 40% and 20% OME_3 showed reductions of 38.4% and 23.3%, respectively. The earlier ignition observed with OME_3 is attributed to its higher cetane number and lower boiling point, a finding also highlighted by Popp et al. [51]. These characteristics improve fuel reactivity and facilitate faster vaporization, enabling the droplet to reach ignition conditions more swiftly. This accelerated evaporation results in a larger fraction of the droplet transitioning to the vapor phase, thereby enhancing premixed combustion and reducing soot formation. While the reduction in ignition delay is influenced by both enhanced volatility (physical effect) and increased fuel reactivity (chemical effect), a strict quantitative separation between these contributions is not possible within the scope of the present experiments. The lower boiling characteristics of OME_3 promote faster droplet heating and vaporization, facilitating rapid formation of a combustible mixture during the pre-ignition phase. Simultaneously, the higher cetane number and inherent oxygen content enhance low-temperature oxidation kinetics, leading to earlier autoignition. The magnitude of reduction suggests that chemical reactivity plays a dominant role, with volatility effects acting as a supporting mechanism. The error bars in Fig. 8 represent the standard deviation from seven replicate tests for each fuel blend, reflecting variation in ignition timing across replicates. The observed variability includes contributions from both measurement uncertainty and slight differences in initial droplet size and positioning on the thermocouple, despite efforts to maintain consistent experimental conditions. Among the fuels, D60-O40 exhibited the lowest variation, with a standard deviation of 4%, while D40-O60 and D80-O20 showed standard deviations of 6% and 7%, respectively, and D100 (pure diesel) showed the highest variability at 8%. Overall, the variability in ignition delay remains within a relatively narrow range (4-8%) across all fuel

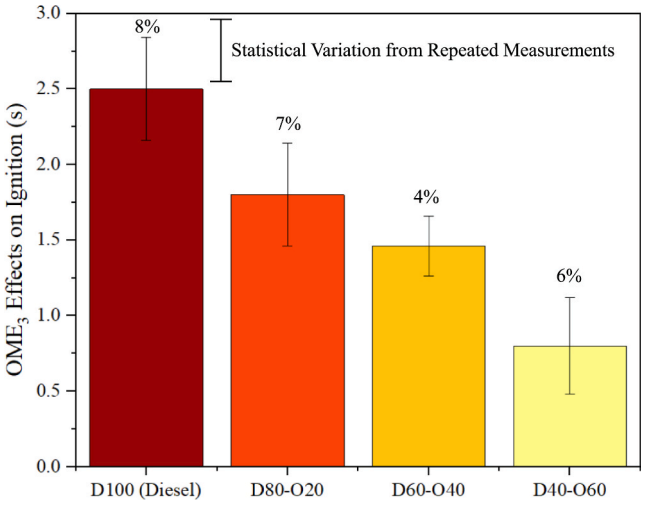

Fig. 8. Comparative ignition delay of diesel-OME_3 blends.

blends, indicating comparable repeatability rather than a significant improvement in ignition consistency with OME_3 addition.

3.6. Droplet Burn Duration

The burn duration of each fuel droplet was defined as the time interval between the onset of ignition and the disappearance of any visible flame, based on high-speed imaging observations. It is important to note that the disappearance of the visible flame does not always coincide exactly with the complete disappearance of the liquid mass (i.e., when the equivalent diameter approaches zero), indicating that non-luminous evaporation or residual fuel may persist beyond visible combustion.

Experimental results indicate that pure diesel (D100) had the shortest burn duration, approximately 1.1 seconds. As the proportion of OME_3 in the fuel blends increased, the burn duration increased. The D80-O20 and D60-O40 blends recorded durations of 1.18 and 1.30 seconds, respectively. The D40-O60 blend exhibited the longest burn duration at 1.41 seconds, representing an approximately 28% increase compared to diesel. This trend indicates that higher OME_3 content promotes longer combustion durations associated with lower heating value and more distributed heat release, supported by its oxygen-rich composition [52]. The shorter ignition delays commonly observed in OME_3-rich blends enable earlier combustion initiation. However, due to OME_3's lower energy density and more distributed heat release, combustion duration is extended, enabling a more complete and efficient burn. The oxygen content of OME_3 enhances oxidation reactions, improving combustion efficiency and reducing soot formation. These findings are consistent with previous research demonstrating enhanced combustion stability and cleaner emissions in oxygenated fuel blends [53,54].

The error bars in Fig. 9 represent the standard deviation across seven replicate tests. D100 and D40-O60 exhibited higher variability, with standard deviations of 8% and 9%, respectively. In contrast, D80-O20 and D60-O40 showed more consistent results, with deviations of 4% and 5%. This suggests that moderate OME_3 addition improves combustion stability, while the slight increase in variability at higher OME_3 concentrations may be attributed to changes in evaporation behavior or fuel-air mixing dynamics.

Overall, the findings indicate that blending diesel with more than 50% OME_3 substantially improves combustion characteristics by reducing ignition time, extending combustion duration, and minimizing soot formation.

4. Conclusions

The evaporation and combustion behavior of diesel and OME_3-diesel blend droplets (D80-O20, D60-O40, and D40-O60) were experimentally investigated using a temperature-controlled optical setup with high-speed imaging. Key parameters, including equivalent droplet diameter (based on projected area), ignition delay, combustion duration, and soot formation, were systematically evaluated.

All fuels exhibited initial thermal expansion followed by vaporization, with increasing OME_3 content promoting faster and more uniform evaporation. Combustion characteristics varied significantly with fuel composition: pure diesel showed delayed ignition, unstable flame behavior, and high soot luminosity, whereas OME_3 blends exhibited earlier ignition, more stable flame development, and reduced visible soot, particularly for D40-O60.

Ignition delay decreased substantially with increasing OME_3 content, with D40-O60 showing an approximate 66% reduction relative to diesel. In contrast, combustion duration increased, reflecting a more distributed heat release process associated with the lower heating value and oxygenated nature of OME_3, rather than a direct enhancement in combustion efficiency.

Soot analysis demonstrated that although visible soot was significantly reduced, the number density of fine particulates increased, with sub-micrometer particle counts rising from approximately 120 to 340-350 particles/mm^2. This indicates a transition from larger soot agglomerates to finer particles due to enhanced oxidation and suppressed particle growth.

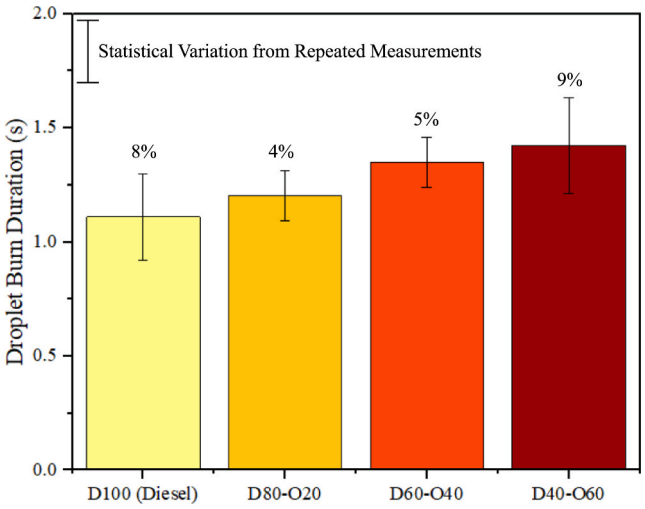

Fig. 9. Comparison of burning durations for diesel-OME_3 droplets.

Overall, OME_3 alters combustion behavior by reducing visible soot emissions while increasing ultrafine particle formation, highlighting the need for further investigation and mitigation strategies for nanoparticle emissions. However, this apparent improvement in visible combustion characteristics is accompanied by an increase in ultrafine particle formation, highlighting a trade-off between reduced soot agglomeration and increased particle number density. This finding underscores the need to consider both emissions quality and quantity when evaluating oxygenated fuel performance.

Future work should focus on detailed burning rate analysis under controlled conditions to enable direct comparison with classical droplet combustion models and support the development of predictive combustion frameworks.

CRediT authorship contribution statement

Farhad Mazari: Writing – original draft. **Thanos Megaritis:** Supervision.

Declaration of competing interest

The authors declare the following financial interests/personal relationships which may be considered as potential competing interests: Farhad Mazari reports financial support was provided by Brunel University London College of Engineering Design and Physical Sciences. If there are other authors, they declare that they have no known competing financial interests or personal relationships that could have appeared to influence the work reported in this paper.

Acknowledgments

The authors gratefully acknowledge financial support from the Engineering and Physical Sciences Research Council (EPSRC), United Kingdom, under Grant No. EP/X019578/1. The authors also acknowledge the facilities and technical support provided by the College of Engineering, Design and Physical Sciences, Brunel University London.

Data availability

Data will be made available on request.

References

[1] Cai L, Sudholt A, Lee DJ, Egolfopoulos FN, Pitsch H, Westbrook CK, et al. Chemical kinetic study of a novel lignocellulosic biofuel: Di-n-butyl ether oxidation in a laminar flow reactor and flames. Combust. Flame 2014;161:798–809.
[2] Zhong A, Han D. Experimental and kinetic modelling studies on di-n-butyl ether low-temperature auto-ignition. Combust. Flame 2022;237:111882.
[3] Sui M, Zhu Z, Li F, Wang H. Effect of ferrocene as a combustion catalyst on the premixed combustion flame characteristics of Jatropha biodiesel. Combust. Flame 2024;259:113180.
[4] Tran L-S, Wullenkord J, Li Y, Herbinet O, Zeng M, Qi F, et al. Probing the low-temperature chemistry of di-n-butyl ether: Detection of previously unobserved intermediates. Combust. Flame 2019;210:9–24.
[5] Natived D, Herzler J, Krzywdziak S, Peukert S, Fikri M, Schulz C. Shock-tube study of the influence of oxygenated additives on benzene pyrolysis: Measurement of optical densities, soot inception times and comparison with simulations. Combust. Flame 2022;243:111985.
[6] Xue T, Liang D, Guo X, Jiang Y, Shen D. Ignition and combustion characteristics of ultrasonically levitated single droplets of nano-boron/oxygenated fuel slurries. Appl. Energy 2024;357:122409.
[7] Klokic S, Hochegger M, Schober S, Mittelbach M. Investigations on an efficient and environmentally benign poly(oxymethylene) dimethyl ether (OME3-5) fuel synthesis. Renewable Energy 2020;147:2151–9.
[8] Preuß J, Munch K, Denbratt I. Performance and emissions of renewable blends with OME3-5 and HVO in heavy-duty and light-duty compression ignition engines. Fuel 2021;303:121275.
[9] Liu Y, Zhang R, Wang C, Chen H, Lyu G, Wang J, et al. Soot particles generated by n-heptane and n-heptane/OME3 in an inverse diffusion flame: A comparative analysis of physical properties and oxidative reactivity. Fuel 2025;394:135097.
[10] Esposito V, Sirignano M. Effect of strain rate on nanoparticles and soot in counterflow flames of ethylene/ethanol and ethylene/OME3. Fuel 2025;379:133094.
[11] Mazari F, Ganippa L, Megaritis T. Characterisation of deposits formed from urea-water-solution droplets under high-temperature engine environment. Fuel 2025;402:135987.
[12] Ghadamkheir K, Zareei J, Yang X, Hatami M. Effects of diesel-OME1 blended fuel on combustion characteristics of a heavy-duty compression ignition engine: A numerical study. Alexandria Eng. J. 2023;64:493–503.
[13] Haspel P, Gierth S, Popp S, Scholtissek A, Rieß S, Wensing M, et al. Large-eddy simulation of OME3 and OME4 spray combustion under heavy-duty conditions. Fuel 2023;353:129097.
[14] Kathrotia T, Bierkandt T, Gaiser N, Richter S, Lindner F, Jacobs S, et al. Combustion kinetics of alternative fuels, Part IV: Extending reaction mechanism "DLR Concise" to include oxygenated components. Combust. Flame 2025;271:113841.
[15] Gaiser N, Bierkandt T, Oßwald P, Zinsmeister J, Kathrotia T, Shaqiri S, et al. Oxidation of oxymethylene ether (OME0-5): An experimental systematic study by mass spectrometry and photoelectron-photoion coincidence spectroscopy. Fuel 2022;313:122650.
[16] Ferraro F, Russo C, Schmitz R, Hasse C, Sirignano M. Experimental and numerical study on the effect of oxymethylene ether-3 (OME3) on soot particle formation. Fuel 2021;286:119353.
[17] De Ras K, Herbinet O, Battin-Leclerc F, Eschenbacher A, Kusenberg M, Varghese RJ, et al. Van Geem, Fundamental investigation of the pyrolysis chemistry of oxymethylene ethers. Part II: Experiments and comprehensive model analysis. Combust. Flame 2025;275:114122.
[18] Asad U, Ramos M, Tjong J. An investigation of OME3-diesel fuel blends on a multi-cylinder compression ignition engine, SAE Tech. Pap. 2022:2022–01-0439.
[19] Mazari F. A study on emission reduction and combustion efficiency, analyzing oxymethylene ether (OME1-5) with diesel fuel. Fuel 2024;375:132578.
[20] He T, Wang Z, You X, Liu H, Wang Y, Li X, et al. A chemical kinetic mechanism for the low- and intermediate-temperature combustion of polyoxymethylene dimethyl ether 3 [PODE3]. Fuel 2018;212:223–35.
[21] Cai L, Jacobs S, Langer R, vom Lehn F, Heufer KA, Pitsch H. Auto-ignition of oxymethylene ethers (OMEn, n = 2-4) as promising synthetic e-fuels from renewable electricity: Shock tube experiments and automatic mechanism generation. Fuel 2020;264:116711.
[22] Pélerin D, Gaukel K, Härtl M, Jacob E, Wachtmeister G. Potentials to simplify the engine system using the alternative diesel fuels oxymethylene ether OME1 and OME3-6 on a heavy-duty engine. Fuel 2020;259:116231.
[23] Wang H, Yao Z, Chen Y, Li B, Zhong X, Zhang M, et al. Combined experimental and kinetic modeling study on the low-temperature oxidation of OME3/n-heptane blends. J. Energy Inst. 2024;114:101633.
[24] Chen Y, Zhong X, Wang H, Li B, Yao Z, Zhang M, et al. Experimental and kinetic modeling study on low-temperature oxidation of gasoline and diesel/polyoxymethylene dimethyl ether (OME3) blends. Combust. Flame 2023;255:112902.
[25] Radaideh MI, Manias DM, Kyritsis DC, Goussis DA. OME2-4/air mixtures: Structure and propagation mechanism of laminar premixed flames. Fuel 2024;363:131004.
[26] Parravicini M, Barro C, Boulouchos K. Compensation for differences in LHV of diesel-OME blends using injector nozzles with different hole numbers: Emissions and combustion. Fuel 2020;259:116166.
[27] Sun Z, Coolen R, Wang Y, Cuijpers M, Somers B, Maes N. Combustion characteristics of oxymethylene dimethyl ether-diesel blends: An experimental investigation using a constant-volume combustion chamber. Fuel 2024;360:130587.
[28] Zacherl F, Wopper C, Schwanzer P, Rabl H-P. Potential of synthetic fuel oxymethylene ether for use in a single-cylinder non-road diesel engine: Thermodynamics and emissions. Energies 2022;15:7932.
[29] Liu Y, Zhang R, Wang J, Wang Y, Lv G, Yang H, et al. Soot particles formed by n-heptane and n-heptane/oxymethylene ether-3 in an inverse diffusion flame: Comparative analysis of chemical features. Fuel 2024;366:131422.
[30] Liang D, Xue T, Li L, Qian Y, Xu W, Lin R, et al. Ignition and combustion properties of ultrasonically levitated single nano-aluminum-based slurry droplets with various liquid oxygenated fuels and solid contents. Combust. Flame 2025;278:114275.
[31] Liang D, Ren K, Wu Z, Jiang Y, Shen D, Li H, et al. Combustion characteristics of oxygenated slurry droplets of nano-Al/EtOH and nano-Al/TPGME blends. Energy 2021;220:119693.
[32] Ibadurrohman IA, Hamidi N, Yuliati L. Winarto, M. Mikami, Enhancement of flame spread and droplet dynamics behavior of biodiesel constituents with ethanol and MWCNT-OH additions, Fuel 2024;358:130100.
[33] Ando S, Nakaya S, Tsue M. Effects of oxidative degradation on single-droplet burning behavior of refined palm and Jatropha curcas oil. Combust. Flame 2024;259:113138.
[34] Xu J, Shi S, Li J, Wang J. Effect of droplet spacing on micro-explosion and combustion characteristics of multi-component fuel droplet clusters. Fuel 2024;373:132323.
[35] Bae JH, Avedisian CT. Experimental study of combustion dynamics of jet fuel droplets with additives in the absence of convection. Combust. Flame 2004;137:148–62.
[36] Ando S, Wu Y, Nakaya S, Tsue M. Droplet combustion behavior of oxidatively degraded methyl laurate and methyl oleate in microgravity. Combust. Flame 2020;214:199–210.
[37] Liu YC, Farouk T, Savas AJ, Dryer FL, Avedisian CT. Spherically symmetric combustion of methyl decanoate droplets and comparison with detailed numerical modeling. Combust. Flame 2013;160:641–55.
[38] Avulapati MM, Megaritis T, Xia J, Ganippa L. Experimental understanding of micro-explosion and puffing dynamics in ternary emulsion droplets. Fuel 2019;239:1284–92.
[39] Avulapati MM, Ganippa LC, Xia J, Megaritis A. Puffing and micro-explosion of diesel-biodiesel-ethanol blends. Fuel 2016;166:59–66.
[40] Fechter M, Haspel P, Hasse C, Braeuer AS. Vapor pressures and latent heats of vaporization of poly(oxymethylene) dimethyl ethers (OME3 and OME4) up to the vicinity of the critical temperature. Fuel 2021;303:121274.
[41] Antonov DV, Fedorenko RM, Strizhak PA. Microexplosion of ternary liquid droplets. Powder Technol. 2025;464:121210.
[42] Pitsch H, Goeb D, Cai L, Willems W. Potential of oxymethylene ethers as renewable diesel substitutes. Prog. Energy Combust. Sci. 2024;104:101173.
[43] Jerzak W. Extinction limits of swirl nonpremixed methane flames and CH/C_xH/N mixtures: Experimental evaluation and thermodynamic calculations. Energy Fuels 2018;32:7179–87.
[44] Nobili A, Frassoldati A, Faravelli T, Cuoci A. Soot formation in combustion of spherically symmetric isolated fuel droplets with different initial diameters. Fuel 2024;363:130403.
[45] Lin Q, Tay KL, Yang W. Auto-ignition of polyoxymethylene dimethyl ether 3 blended with diesel and gasoline under homogeneous charge compression ignition. Energy Convers. Manag. X 2021;11:100093.
[46] Goroshin S, Palečka J, Bergthorson JM. Fundamental aspects of laminar flames in nonvolatile solid fuel suspensions. Prog. Energy Combust. Sci. 2022;91:100994.
[47] García-Oliver JM, Novella R, Micó C, Bin-Khalid U. Numerical investigation of oxymethylene ether-diesel blends for soot reduction in compression ignition engines. Fuel 2022;324:124768.
[48] Aggarwal SK. Single droplet ignition: Theoretical analyzes and experimental findings. Prog. Energy Combust. Sci. 2014;45:79–107.
[49] Ilbas M, Kumuk O, Karyeyen S. Modelling of gas-turbine colorless distributed combustion with hydrogen-enriched kerosene fuel. Int. J. Hydrogen Energy 2022;47:12354–64.
[50] Farooq MS, Baig A, Wei Y, Liu H, Ali U. Review of developments addressing cold-start challenges in methanol-fueled spark ignition engines. Int. J. Hydrogen Energy 2025;99:852–71.
[51] Popp T, Lechner R, Becker M, Hebauer M, O'Connell N, Brautsch M. Potentials of OME/diesel blends for stationary power production: Improving emission characteristics of a diesel CHP unit. Appl. Therm. Eng. 2019;153:483–92.
[52] Holzer A, Günthner M, Jung P. Performance of pure OME and HVO-OME blends as alternative fuels for diesel engines. Automot. Engine Technol. 2022;7:369–83.
[53] Lucas SP, Zdanowicz AJ, Wolff WW, Windom BC. Combustion characteristics of diisopropoxymethane, a low-reactivity oxymethylene ether. Fuel 2024;362:130727.
[54] Sun Z, van Beers H, Cuijpers M, Somers B, Maes N. Design-of-experiments optimized OMEx-diesel blends for heavy-duty engines -Part 1: Combustion and emissions with EGR and injection timing variation. Fuel 2025;381:133392.